frontiers in Energy Research

ORIGINAL RESEARCH
published: 17 July 2020
doi: 10.3389/fenrg.2020.00128

High-Purity and Clean Syngas and Hydrogen Production From Two-Step CH_4 Reforming and H_2O Splitting Through Isothermal Ceria Redox Cycle Using Concentrated Sunlight

Srirat Chuayboon[1], *Stéphane Abanades*[2]* *and Sylvain Rodat*[2]

[1] Department of Mechanical Engineering, King Mongkut's Institute of Technology Ladkrabang, Chumphon, Thailand,
[2] Processes, Materials, and Solar Energy Laboratory, PROMES-CNRS, Font-Romeu, France

OPEN ACCESS

Edited by:
Yu Luo,
Fuzhou University, China

Reviewed by:
Muhammad Aziz,
The University of Tokyo, Japan
Cheng Tung Chong,
Shanghai Jiao Tong University, China

***Correspondence:**
Stéphane Abanades
stephane.abanades@promes.cnrs.fr

Specialty section:
This article was submitted to Hydrogen Storage and Production, a section of the journal Frontiers in Energy Research

Received: *23 March 2020*
Accepted: *27 May 2020*
Published: *17 July 2020*

Citation:
Chuayboon S, Abanades S and Rodat S (2020) High-Purity and Clean Syngas and Hydrogen Production From Two-Step CH_4 Reforming and H_2O Splitting Through Isothermal Ceria Redox Cycle Using Concentrated Sunlight. Front. Energy Res. 8:128. doi: 10.3389/fenrg.2020.00128

The thermochemical conversion of methane (CH_4) and water (H_2O) to syngas and hydrogen, via chemical looping using concentrated sunlight as a sustainable source of process heat, attracts considerable attention. It is likewise a means of storing intermittent solar energy into chemical fuels. In this study, solar chemical looping reforming of CH_4 and H_2O splitting over non-stoichiometric ceria ($CeO_2/CeO_{2-\delta}$) redox cycle were experimentally investigated in a volumetric solar reactor prototype. The cycle consists of (i) the endothermic partial oxidation of CH_4 and the simultaneous reduction of ceria and (ii) the subsequent exothermic splitting of H_2O and the simultaneous oxidation of the reduced ceria under isothermal operation at ∼1,000°C, enabling the elimination of sensible heat losses as compared to non-isothermal thermochemical cycles. Ceria-based reticulated porous ceramics with different sintering temperatures (1,000 and 1,400°C) were employed as oxygen carriers and tested with different methane flow rates (0.1–0.4 NL/min) and methane concentrations (50 and 100%). The impacts of operating conditions on the foam-averaged oxygen non-stoichiometry (reduction extent, δ), syngas yield, methane conversion, solar-to-fuel energy conversion efficiency as well as the effects of transient solar conditions were demonstrated and emphasized. As a result, clean syngas was successfully produced with H_2/CO ratios approaching 2 during the first reduction step, while high-purity H_2 was subsequently generated during the oxidation step. Increasing methane flow rate and CH_4 concentration promoted syngas yields up to 8.51 mmol/g_{CeO_2} and δ up to 0.38, at the expense of enhanced methane cracking reaction and reduced CH_4 conversion. Solar-to-fuel energy conversion efficiency, namely, the ratio of the calorific value of produced syngas to the total energy input (solar power and calorific value of converted methane), and CH_4 conversion were achieved in the range of 2.9–5.6% and 40.1–68.5%, respectively.

Keywords: methane reforming, ceria foam, redox cycle, concentrated solar power, hydrogen, syngas, H_2O splitting

INTRODUCTION

Most hydrogen production is currently achieved via conventional steam reforming of natural gas (Equation 1) (Zheng Q. et al., 2014). The resulting product is syngas (H_2+CO), and then water–gas shift reaction is applied to convert the produced CO into H_2 and CO_2, thus contributing to greenhouse gas emissions. The reaction is endothermic, requiring heat to be supplied to the process for reactions in the temperature range 700–1,000°C (Zheng Q. et al., 2014). In general, the heat source is provided by combustion of up to 41% of the methane feedstock, causing 24% reduction in product energy content compared to the feedstock (Simakov et al., 2015; Krenzke et al., 2017), and costly catalysts are necessary to conduct such reactions (Dincer and Rosen, 2013). This unavoidably results in a significant portion of methane feedstock consumption, as well as greenhouse gas emissions (especially CO_2), which contribute to climate change and global warming (Nejat et al., 2015).

$$\text{Conventional steam reforming}: \quad CH_4 + H_2O \rightarrow 3H_2 + CO \ \Delta H^0 = +206\text{kJ/mol} \quad (1)$$

Alternatively, the partial oxidation of methane through metal oxide redox cycle (namely, chemical looping reforming of methane, CLRM) is a promising pathway to produce clean syngas and high-purity hydrogen (Di et al., 2019). This reaction encompasses two steps: (1) endothermic partial oxidation of methane along with metal oxide reduction to produce clean syngas and (2) exothermic re-oxidation of the oxide with steam (or CO_2) to produce high-purity H_2 (or CO). The net products of CLRM are the same as those of steam reforming (Equation 1). The advantages of CLRM through metal oxides over the conventional methane reforming process are (i) the syngas is produced with a H_2:CO ratio of 2:1 during the first step, suitable for methanol synthesis (Otsuka et al., 1998), (ii) an excess in oxidizer is not necessary, while a conventional process needs to be operated with excess steam (H_2O:$CH_4 \geq 3$) (Simakov et al., 2015), which raises energy requirements and reduces process efficiency, (iii) catalysts are not required, and (iv) an isothermal operation between both steps is possible; therefore, the temperature swing between the reduction and the oxidation steps can be avoided (Chuayboon et al., 2019a), thereby resulting in fast and continuous process operation (no time wasted for cooling down to oxidation temperature) and lower sensible heat losses, thus improving the energy conversion efficiency. Among a variety of potential metal oxides (either volatile or non-volatile), cerium oxide [either pure ceria (Chueh et al., 2010; Furler et al., 2014; Marxer et al., 2017; Haeussler et al., 2019) or ceria-based (Otsuka et al., 1999; Zheng Y. et al., 2014; Zhu et al., 2014; Bhosale et al., 2019)] is a particularly attractive candidate given its various beneficial physical and chemical properties. For example, ceria keeps a stable cubic fluorite structure during large changes in oxygen non-stoichiometries (reduction extents; Nair and Abanades, 2016) and exhibits rapid oxygen storage/release through lattice transfer (Furler et al., 2014). Marxer et al. (2017) tested the thermochemical splitting of CO_2 using a pure ceria reticulated porous structure and reported that 100% CO selectivity and 83% molar conversion were achieved. Besides that, 500 consecutive redox cycles were conducted under the same experimental conditions to validate pure ceria stability and structural robustness. A study on the different dopants to ceria (ceria-based ceramics) for two-step thermochemical splitting of H_2O/CO_2 was achieved to improve its stability as well as redox activity (Bhosale et al., 2019). Zhu et al. (2014) studied CLRM over a CeO_2-Fe_2O_3 oxygen carrier and found that this material displayed great performance, thanks to the chemical interaction between Ce and Fe species. The presence of CeO_2, Fe_3O_4, and $CeFeO_3$ formed in the recycled samples was reported. The reactions of CLRM over ceria include the following steps:

First step: the endothermic reduction reaction of ceria and simultaneous partial oxidation of methane is given in Equation (2).

$$CeO_2 + \delta CH_4 \rightarrow \ CeO_{2-\delta} + \delta CO + 2\delta H_2 \quad (2)$$

Second step: the exothermic oxidation reaction of oxygen-deficient ceria with H_2O is given in Equation (3).

$$CeO_{2-\delta} + \delta H_2O \ \rightarrow \ CeO_2 + \delta H_2 \quad (3)$$

During the reduction step (Equation 2), the amount of released oxygen from ceria (δ_{red}) is calculated by the summation of the mole amounts of CO (main product), CO_2, and H_2O according to Equation (4).

$$\delta_{red} = \frac{n_{CO} + 2n_{CO_2} + n_{H_2O}}{n_{CeO_2}} \quad (4)$$

where n_i is the mole amount of species i.

During the oxidation step (Equation 3), the amount of oxygen uptake (δ_{ox}) is calculated from the total amount of H_2 produced minus the amount of H_2 produced by the side reactions with respect to the carbon gasification reaction [namely, the carbon produced from methane thermal dissociation, $CH_4 \rightarrow C + 2H_2$, during the previous reduction step is gasified with water ($C + H_2O \rightarrow CO{+}H_2$ and $C{+}2H_2O{\rightarrow}CO_2{+}2H_2$), producing additional CO, CO_2, and H_2] according to Equation (5).

$$\delta_{ox} = \frac{n_{H_2} - n_{CO} - 2n_{CO_2}}{n_{CeO_2}} \quad (5)$$

To quantify how much injected CH_4 is converted to the products regarding syngas, solid carbon, or soot, CH_4 conversion is calculated by Equation (6).

$$X_{CH_4} = 1 - \frac{\dot{m}_{unreacted\ CH_4}}{\dot{m}_{CH_4}} \quad (6)$$

X_{CH_4} is the methane conversion, $\dot{m}_{unreacted\ CH_4}$ is the mass flow rate of unreacted methane in the off-gas, and $\dot{m}_{CH_4}$ is the mass flow rate of injected methane.

The solar-to-fuel energy conversion efficiency ($\eta_{solar-to-fuel}$) indicates how well the solar energy is stored into chemical products. It is defined as the ratio of the calorific value of syngas produced by ceria redox cycle to the total energy input, which

is the sum of the calorific value of converted methane and solar power in both the reduction and the oxidation steps, according to Equation (7).

$$\eta_{\text{solar-to-fuel}} = \frac{\left(\dot{m}_{H_2} \cdot LHV_{H_2} + \dot{m}_{CO} \cdot LHV_{CO}\right)_{cycle}}{\dot{P}_{solar} + \left(X_{CH_4} \cdot \dot{m}_{CH_4} \cdot LHV_{CH_4}\right)} \quad (7)$$

where LHV_{H_2}, LHV_{CO}, and LHV_{CH_4} are the lower heating values (J/kg) of H_2, CO, and CH_4, respectively, $\dot{m}_{H_2}$ and $\dot{m}_{CO}$ are the mass flow rates (kg/s) of H_2 and CO produced in the cycle, $\dot{m}_{CH_4}$ is the mass flow rate of injected methane, and $\dot{P}_{solar}$ is the total solar power input (W).

Otsuka et al. (1993) first conducted partial oxidation of methane with ceria in an electrical furnace at 873–1,073 K, and such reaction was accelerated in the presence of Pt black (1 wt%). As a result, the produced syngas with a H_2/CO ratio of 2 and the reduced ceria oxidation with CO_2 were demonstrated. They also reported that, in the CLRM process, an excess in oxidizer was not required as carbon deposition can be precluded by limiting the reduction extent of the metal oxides (Otsuka et al., 1999). Then, the processes were coupled with concentrating solar power technologies (Abanades and Flamant, 2006; Chuayboon et al., 2020). The heat required for such endothermic reactions is thus supplied by concentrated sunlight. This offers an attractive approach to convert intermittent solar energy into storable and dispatchable chemical fuels (Nair and Abanades, 2016) as well as to eliminate CO_2 emissions from feedstock combustion, thereby offering clean and sustainable fuel production. **Figure 1** presents the concept of two-step solar redox cycle with ceria porous foam reduction coupled to partial oxidation of methane (reduction step) and H_2O splitting during oxidation reaction (oxidation step). Concentrated solar energy is used as the process heat source to drive the endothermic reaction during the reduction step and also to maintain the temperature during the oxidation step for isothermal cycle at 1,000°C ($T_{\text{reduction}} = T_{\text{oxidation}}$). Furler et al. (2012) reported that ceria-reticulated porous foam enabled the effective volumetric absorption of concentrated sunlight and efficient heat transfer to the whole reacting structure. However, the optical thickness of the porous ceria structure needs to be properly optimized without hindering the specific surface area and density (material loading) since enhancing the latter properties adversely results in high radiative opacity and eventually causes the temperature gradient issue.

Solar CLRM over ceria has been studied both thermodynamically (Krenzke and Davidson, 2014) and experimentally (Welte et al., 2017). Krenzke and Davidson (2014) thermodynamically examined the CLRM with ceria and reported that combining the partial oxidation of methane with ceria allows isothermal cycling at temperatures as low as 1,223 K, with production of high-quality syngas during the reduction step. However, it was found that thermodynamics predicted solar-to-fuel energy conversion efficiency of 40%, significantly

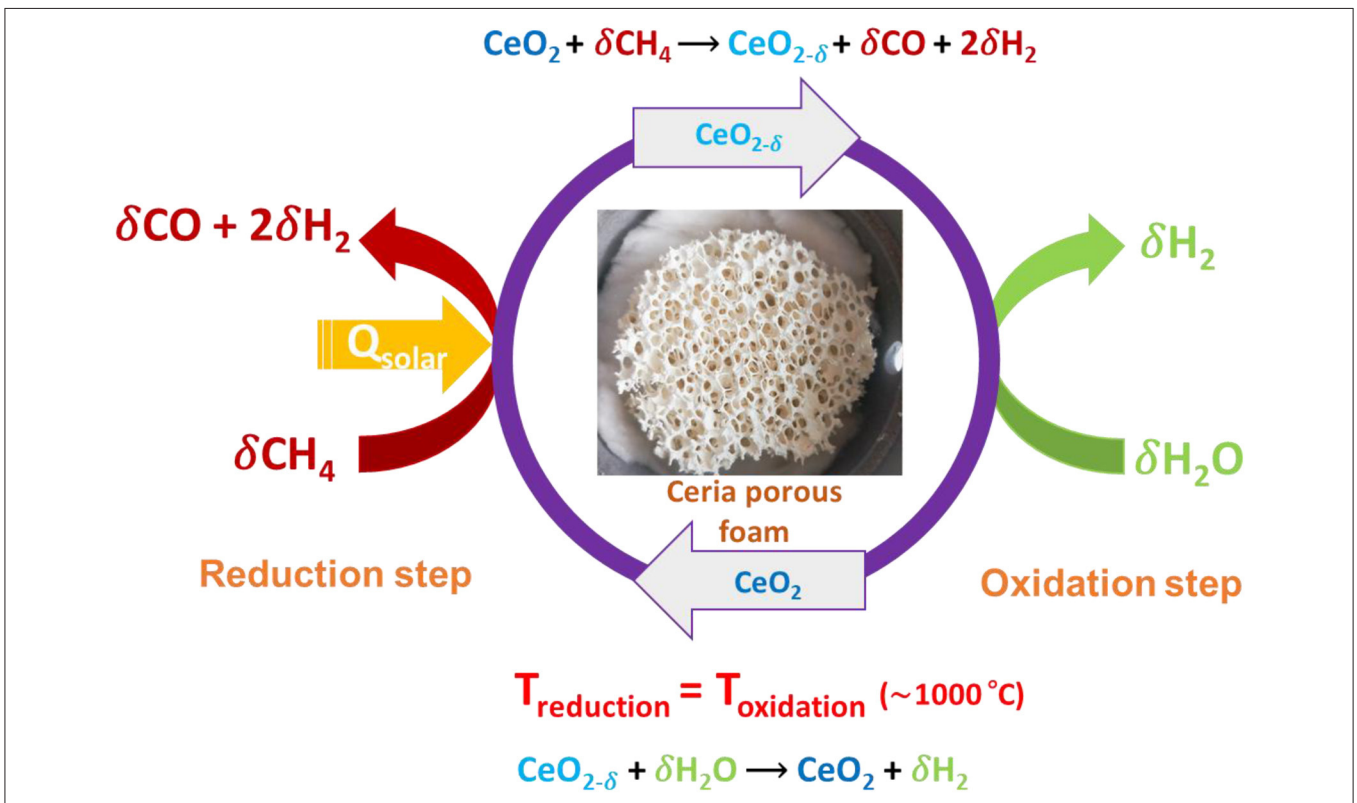

FIGURE 1 | Ceria two-step redox cycle with ceria reduction coupled to the partial oxidation of methane (reduction step) and H_2O splitting during the oxidation reaction (oxidation step).

higher than the reported projected ones (e.g., 27%; Krenzke et al., 2016). Then, the same group (Hathaway et al., 2015; Fosheim et al., 2019) studied solar CLRM with CO_2 over ceria in a prototype reactor operated in a high-flux solar simulator. A fixed bed of ceria particles was placed inside six tube assemblies in the reactor. Then, the cycle was carried out by alternating the flow between CH_4 and CO_2. They reported that a higher temperature favors better performance, and the energetic upgrade factor and the solar-to-fuel energy conversion efficiency were 1.10 and 7%, respectively.

Welte et al. (2017) tested CLRM with ceria particles in a particle transport reactor, either in co-current or counter-current to a CH_4 flow, driven by a solar simulator. Methane conversions up to 89% at 1,300°C for residence times below 1 s and maximum extent of ceria reduction of $\delta = 0.25$ were mentioned. The solar-to-fuel energy conversion efficiency reached 12%, and the produced syngas was solar-upgraded by 24% compared to feedstock. However, it should be noted that the amount of unreacted ceria exiting the reactor was significant.

Warren et al. (2017) investigated the cycle thermodynamics in comparison with the experimental investigation of the partial oxidation of methane over ceria. A theoretical solar-to-fuel conversion efficiency over 45% (with no heat recuperation) was claimed, while experimental solar-to-fuel conversion efficiencies of 9.82% (Warren et al., 2017) and later 10.6% (Warren et al., 2020) were obtained in a packed-bed-type solar reactor using solar simulator as heat source. The same research group also explored the kinetics of the partial oxidation of methane over ceria as performed under atmospheric pressure between 750 and 1,100°C using a thermogravimetric analyzer (Warren and Scheffe, 2018, 2019). The reaction kinetics were studied, and the activation energy was obtained by Arrhenius-type plots as a function of reactant composition. It was found that the activation energy varied with reaction extent between 20 and 80 kJ/mol, rising mostly for large reduction extents ($\delta > 0.15$).

In accordance with prior thermodynamic studies and lab-scale experiments, it was demonstrated that solar CLRM over ceria (as particles or ceramic foam) is of particular interest. However, the reported performance was dependent on the reactor concept, design, and technology. Most of previous studies were likewise focused on thermodynamics (Krenzke and Davidson, 2014; Warren et al., 2017) and experiments (Krenzke et al., 2016; Warren et al., 2020) in small-scale reactors using electrical furnaces or solar simulators as the external heat source instead of real concentrated sunlight. Therefore, this present study aims to further examine the isothermal CLRM and H_2O splitting over tailor-made ceria porous foams in a scalable prototype solar reactor (1.5 kW_{th}) using a real solar concentrating system. The performance of this novel reactor was experimentally assessed, and the impact of transient solar radiation conditions was additionally evaluated. The influence of operating parameters considering CH_4 concentration, methane flow rate, and annealing temperature of ceria foam on thermochemical performance in a 1.5-kW_{th} volumetric solar reactor prototype was evaluated and demonstrated.

MATERIALS AND METHODS

A schematic diagram and a photograph of the 1.5 kW_{th} prototype volumetric solar reactor and auxiliary components are presented in **Figure 2**. The solar reactor is heated by

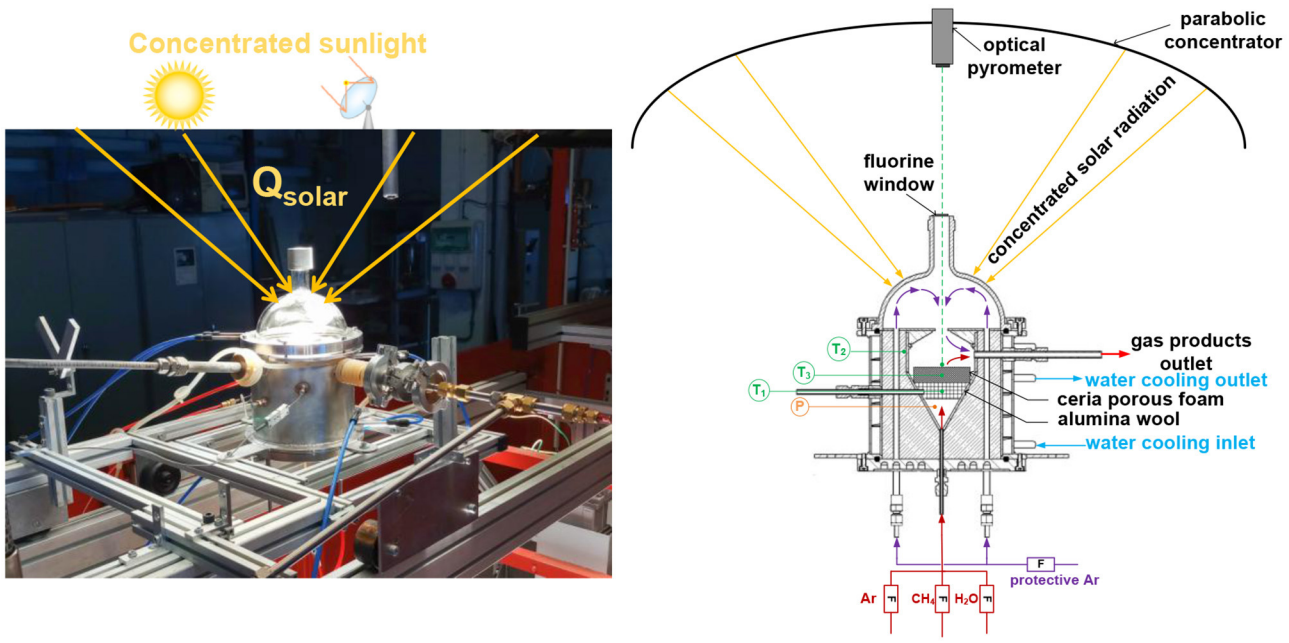

FIGURE 2 | Photograph **(left)** and schematic illustration **(right)** of the 1.5-kW_{th} prototype solar reactor driven by real high-flux solar radiation for methane reforming and H_2O splitting over the ceria redox cycle.

highly concentrated sunlight, delivered by a 2-m-diameter parabolic concentrator with a solar concentration ratio up to 10,551 suns [0.85 m focal distance, peak flux density of ∼10.5 MW/m^2 for a Direct Normal Irradiation (DNI) of 1 kW/m^2] and positioned above the reactor. More details on this solar reactor concept and design have been described previously (Chuayboon et al., 2019b). Three temperature measurements (B-type thermocouples) are installed inside the reactor cavity (T_1 inside alumina wool and T_3 inside ceria porous foam) and at the external cavity wall surface (T_2). A solar-blind pyrometer placed at the center of the facedown parabolic concentrator also measures the temperature inside the cavity receiver to compare it with T_1 and T_3. In addition, one pressure sensor is used to measure the pressure in the reactor cavity (P).

Two reactive ceria porous foams were synthesized via replication technique (Furler et al., 2012) using polymer scaffolds as templates, and their physical properties are shown in **Table 1**. The first ceria foam was annealed at 1,000°C for 6 h (labeled as CeF-1000), while the other was annealed at 1,000°C for 6 h and then at 1,400°C for 2 h (labeled as CeF-1400).

The ceria porous foam was placed on the alumina wool support inside the volumetric ceramic cavity (metallic alloy, volume: 0.3 L and total height: 115 mm). The reactor was positioned at the focal point of the high flux solar concentrator. It was then heated by concentrated sunlight, while the solar heating rate was adjusted manually using the shutter opening system. **Figure 3** shows a representative transient solar power and DNI evolution during both solar heating and isothermal ceria reduction with methane, followed by reduced ceria oxidation with water in the solar reactor (cycle #1, ceria foam CeF-1400, mass 30.963 g). During solar heating (0–45 min), a fluctuation in DNI was evidenced because of transient cloud passage, especially in the morning (10:00–11:00 am). During isothermal ceria reduction with methane, solar power input was adjusted by the shutter to 730 W at t = 45–55 min (at the beginning of reaction) and increased to 900 W at t = 55 min in order to compensate for the endothermic reaction and solar transients, with the objective to maintain the isothermal operation at 1,000°C. During oxidation, both solar power input and DNI were quite stable at 900 W and 1,037 W/m^2 after some transients at the beginning of the period. These variations highlighted the instabilities of real solar power input, which challenged the control of the operating temperature for isothermal operation during on-sun testing.

TABLE 1 | Physical properties of ceria foams.

Number	Annealing temperatute (°C)	Label	Initial ceria mass (g)	Pore size density (pore per inch)	Specific surface area (m^2/g)	Mean cell size (mm)	Apparent density (g/cm^3)	Apparent porosity (%)
1	1,000	CeF-1000	18.371	10	<1	3.5	0.595	91.8
2	1,400	CeF-1400	30.963	13	<1	2.5	0.780	89.1

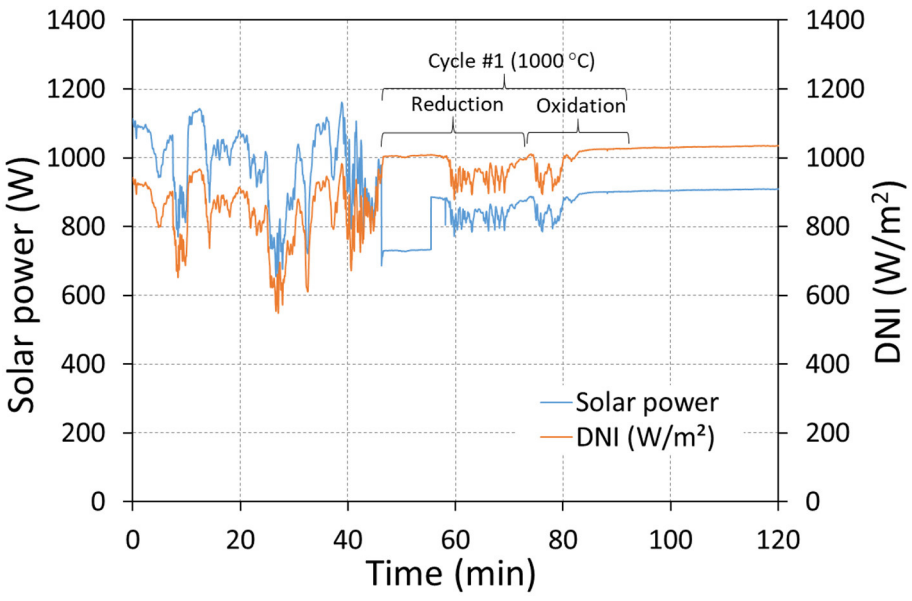

FIGURE 3 | Solar power and direct normal irradiation evolution in the reactor during the heating phase, ceria foam reduction with methane and oxidation with H_2O (CeF-1400: mass 30.963 g, cycle #1).

Figure 4 reveals homogeneous temperatures across the ceria-reticulated porous foam, as evidenced by a minimal gap between the top foam surface temperature ($T_{pyrometer}$), middle temperature (T_3), and temperature at the bottom of the foam (T_1). In addition, the external cavity wall surface temperature of the reactor cavity receiver (T_2) was slightly lower than $T_{pyrometer}$, thereby indicating the uniform solar radiative absorption across the reactive volumetric porous absorber and the solar reactor. This is because the ceria foam exhibits low opacity, while the reactor features high volumetric incident thermal radiation absorption, thus allowing solar energy to penetrate more homogeneously through the foam and reactor cavity receiver. Besides that, the cavity pressure was stable at 0.86 bar during solar heating and rose to 0.90 bar as the reaction progressed (P_{atm} = 0.86 bar at site elevation). During both steps, the temperatures, especially T_3, were quite constant at around 1,000°C, demonstrating isothermal operation and satisfying temperature control in case of small DNI variations.

Once the targeted temperature was stabilized at 1,000°C, the CH_4 flow (in the range of 0.1–0.4 NL/min) was introduced along with Ar carrier gas (0.2 NL/min) at the cavity bottom until the reduction reaction was finished. Then, H_2O (0.2 g/min) was introduced along with Ar carrier gas (0.2 NL/min) for a subsequent oxidation step (liquid water was injected via a stainless steel capillary at the cavity bottom, thanks to a devoted liquid mass flow controller, and was subsequently vaporized when exiting the tube outlet). During reactor heating and reaction proceeding, Ar protective gas flows (2 NL/min) were supplied to protect the transparent window as well as to sweep product gases exiting via the outlet. The produced gases (H_2, CO, CO_2, H_2O, and CH_4 for methane-promoted redox cycle) exited the reactor via its outlet port and were then cleaned by both the gas scrubbing system and the filtering unit (in which the H_2O produced and some soot were trapped) prior to gas analysis. After that, they were continuously analyzed via online gas analyzers (thermal conductivity detector for H_2 and infrared sensors for CO, CO_2, and CH_4, calibrated with standard gases). The averaged oxygen non-stoichiometry of $CeO_{2-\delta}$ (δ), fuel yields, gas production rates, CH_4 conversion, and solar-to-fuel energy conversion efficiency were experimentally examined and compared. The outlet flow rate of each product gas species (F_i) was determined using their measured transient mole fraction (y_i) and the known total inlet Ar flow rate (F_{Ar}): ($F_i = F_{Ar} \cdot y_i / y_{Ar}$). In addition, the syngas yields from each reaction were calculated separately. For example, the gases produced from the main reactions regarding both partial reduction of ceria by methane (Equation 2) and ceria oxidation (Equation 3) and from the side reactions regarding both the H_2 produced by methane cracking ($CH_4 \rightarrow 2H_2 + C$) and the gases produced from C deposit gasification with steam during oxidation ($C + H_2O \rightarrow CO + H_2$ and $C + 2H_2O \rightarrow CO_2 + 2H_2$) were presented independently in order to highlight the impact of operating conditions on the possible reactions during cycles.

RESULTS AND DISCUSSION

Thermodynamic Analysis

Figure 5 shows the thermodynamic equilibrium composition during the endothermic reduction of ceria and the simultaneous partial oxidation of methane as a function of temperature at 1 bar. With increasing temperature, CH_4 is thermally decomposed to H_2(g) and solid carbon, and CeO_2 is simultaneously reduced

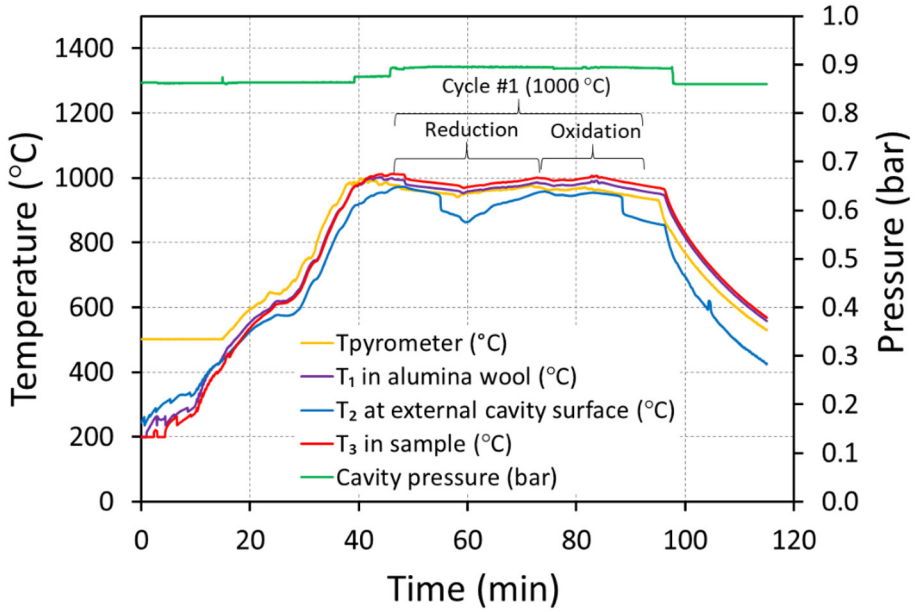

FIGURE 4 | Temperature and pressure evolution in the reactor during the heating phase, ceria foam reduction with methane and oxidation with H_2O (CeF-1400: mass 30.963 g, cycle #1).

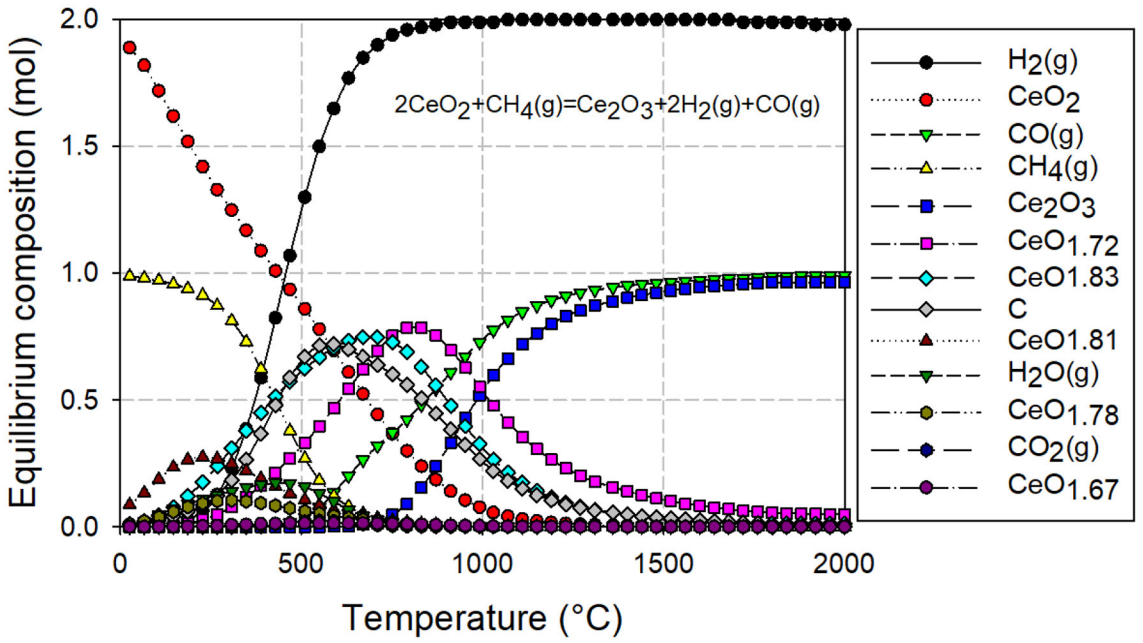

FIGURE 5 | Thermodynamic equilibrium composition of ceria reduction with methane as a function of temperature at 1 bar.

by reactive methane gas (solid–gas reaction), thereby releasing the oxygen from the structure, while partially reduced ceria species ($CeO_{1.81}$ and $CeO_{1.78}$) are formed. Meanwhile, the formation of both H_2O(g) and CO_2(g) in small amounts is observed. At above 500°C, the carbon deposition associated with CH_4 dissociation reacts with the oxygen discharged from ceria, forming CO as well as creating the ceria oxygen vacancies, which is in agreement with previous studies (Krenzke and Davidson, 2014; Warren et al., 2017). The intermediate species of ceria regarding $CeO_{1.72}$, $CeO_{1.83}$, and $CeO_{1.67}$ are produced in negligible amounts, demonstrating the overall possible reduction mechanism occurring during Ce(IV) reduction to Ce(III). At above 1,000°C, the completion of the reaction is approached, resulting in Ce_2O_3, H_2, and CO (with the H_2/CO ratio approaching 2).

Effect of Methane Concentration

The effect of methane concentration on syngas production from ceria foam [mass, 30.9630 g; annealed at 1,400°C (CeF-1400)] was examined for three cycles. **Figure 6** shows the evolution of syngas species production rates and temperatures [inside sample (T_3) and upper surface sample ($T_{pyrometer}$)] as a function of time during ceria reduction (50% CH_4 concentration for cycle #1 and cycle #2 and 100% CH_4 concentration for cycle #3), followed by exothermic ceria oxidation with H_2O (0.2 g/min, 55% steam concentration for three cycles) at the isothermal temperature of 1,000°C. The variations of the syngas production rates and temperatures provided insights into the chemical reaction behavior and associated mechanism.

At cycle #1 during the reduction step (**Figure 6A**), a high-quality and energy-rich syngas was produced, with the H_2/CO molar ratio approaching 2. The maximum of CO_2 production rate of 0.04 NL/min was evidenced at the initial stage, occurring just after CH_4 injection. In fact, the H_2O production rate (theoretically doubling the CO_2 production rate, according to the following reaction: $4CeO_2 + \delta CH_4 \rightarrow 4CeO_{2-\delta} + \delta CO_2 + 2\delta H_2O$) could also be observed according to thermodynamic analysis (**Figure 5**) and previous studies (Krenzke et al., 2016; Nair and Abanades, 2016). The presence of H_2O and CO_2 at the initial state of reaction was due to the large amount in the available surface oxygen that reacts with CH_4 to form both H_2O and CO_2. However, the H_2O production rate cannot be measured from gas analysis since the steam was trapped in the gas scrubbing system before the gas analysis. The CH_4 trend was inverse compared to those of H_2 and CO production rates because of concomitant CH_4 consumption. After the ceria reduction was completed (depletion of available oxygen inside the ceria structure), the syngas production then decreased progressively. At the end of the reaction, CO decreased steadily while H_2 tended to remain stable, because of the CH_4 cracking reaction. Indeed when a lack of oxygen occurs at the ceria surface compared to the constant methane feeding rate, carbon deposition is became faster, which is increasingly favored as oxygen is being depleted during the ceria reduction progress. When the CO production rate approached zero, the CH_4 flow was subsequently stopped. During subsequent oxidation (**Figure 6B**), a sharp increase in H_2 (0.2 NL/min peak production rate) with high purity was evidenced, thanks to fast oxidation kinetics, followed by CO (peak rate, 0.04 NL/min) and CO_2 (peak rate, 0.02 NL/min) production, which arise from the gasification of carbon deposition (stemming from CH_4 cracking in the first step).

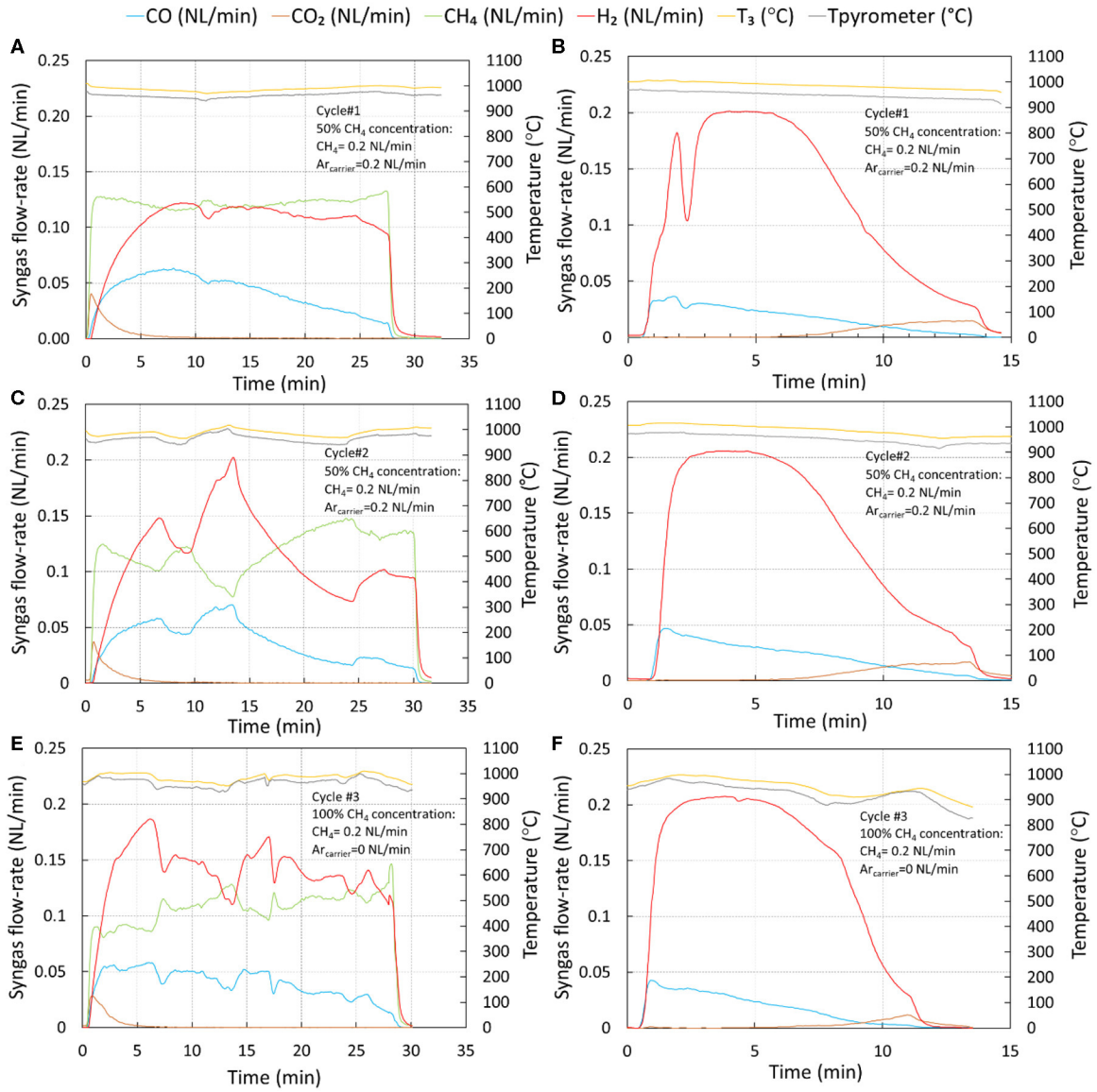

FIGURE 6 | Syngas production rates and reactor temperatures (T_3 and $T_{pyrometer}$) during **(A,C,E)** ceria reduction with CH_4 and **(B,D,F)** reduced ceria oxidation with H_2O for three cycles with different CH_4 concentrations of 50 and 100% at 1,000°C.

At cycle #2, the experiment was repeated with the same operating parameters as for cycle #1 for both steps. As a result, during reduction (**Figure 6C**), a fluctuation in syngas and CH_4 flow rates was noticed. This variation can be explained by the fact that the reactor was sometimes heated at above 1,000°C due to the difficulty to control the temperature over 30 min with the manual shutter opening control system, as reflected by T_3 and $T_{pyrometer}$ fluctuations around the setpoint. As shown in **Figure 6C**, the trends of H_2 and CO production rates were always consistent with those of the temperatures, demonstrating the strong influence of temperature on ceria reduction reaction. Controlling the operating temperature stably throughout the test is therefore necessary. Moreover, it is important to note that the peaks of both H_2 and CO were always occurring slightly after the peak of temperature. For example, in **Figure 6C**, the peak temperature was at 13 min 13 s, while the peaks of H_2 and CO were at 13 min 47 s, which means a 34-s delay, and denoting a small inertia of the reactions. At the final state after a 25-min duration, a plateau region in syngas and CH_4 evolution was evidenced due to the thermally favorable CH_4 cracking reaction caused by solar overheating (>1,000°C). During the oxidation step (**Figure 6D**), the H_2 peak production rate increased up to 0.21 NL/min, while the CO and CO_2 peak production rates were 0.05 and 0.02 NL/min, thus slightly higher than those measured in cycle #1, confirming the stronger effect of CH_4 cracking reaction during the reduction step.

At cycle #3 during reduction (**Figure 6E**), CH_4 concentration was increased to 100% (CH_4 flow rate = 0.2 NL/min without Ar carrier gas at the bottom inlet). Similar to the previous cycle, the syngas and CH_4 production rates still varied in relation to a change in temperature, implying a significant temperature effect on possible reactions. The difference of syngas production rate between 50% (cycle #2) and 100% (cycle #3) methane concentration was not obvious. However, H_2 trend seemed to be higher, while CO trend seemed to be similar as compared to those obtained from cycle #2. In addition, the nominal gas residence time (calculated from the volume of the cavity divided by the total outlet gas flow rate) was 1.87 s at 100% CH_4 concentration compared to 1.70 s at 50% CH_4 concentration, which may in turn promote CLRM over ceria. During oxidation (**Figure 6F**), the peak H_2 production rate was found to be the same as in cycle #2 (0.21 NL/min), but the peak CO (0.04 NL/min) and CO_2 (0.01 NL/min) production rates were lower compared to those in cycle #2, possibly because of a decline in temperature after a 5-min duration (below 1,000°C), which lowers the endothermic carbon gasification reactions ($C + H_2O \rightarrow CO + H_2$). This might lead to solid carbon remaining inside the reactor cavity receiver.

Figure 7 presents the syngas yields during the (a) reduction and the (b) oxidation steps, quantified by time integration of the syngas production rates according to **Figure 6**. During the reduction step at 50% of CH_4 concentration (**Figure 7A**), the H_2 yield (from CH_4 cracking) from cycle #2 was considerably higher [1.72 (cycle #2) vs. 0.88 mmol/g_{CeO_2} (cycle #1)], thus confirming increased thermal CH_4 decomposition due to overheating as mentioned before. In contrast, the CO_2 yield was lower [0.13 mmol/g_{CeO_2} (cycle #1) vs. 0.10 mmol/g_{CeO_2} (cycle#2)], which is attributed to the fresh ceria foam that released more oxygen, as reflected by the highest δ_{red} (0.37). Besides that, both H_2 (from $CeO_2 + CH_4$) and CO (from $CeO_2 + CH_4$) yields remained similar between cycle #1 and cycle #2, demonstrating syngas production yield repeatability. When increasing the CH_4 concentration to 100% (cycle #3), a significant increase

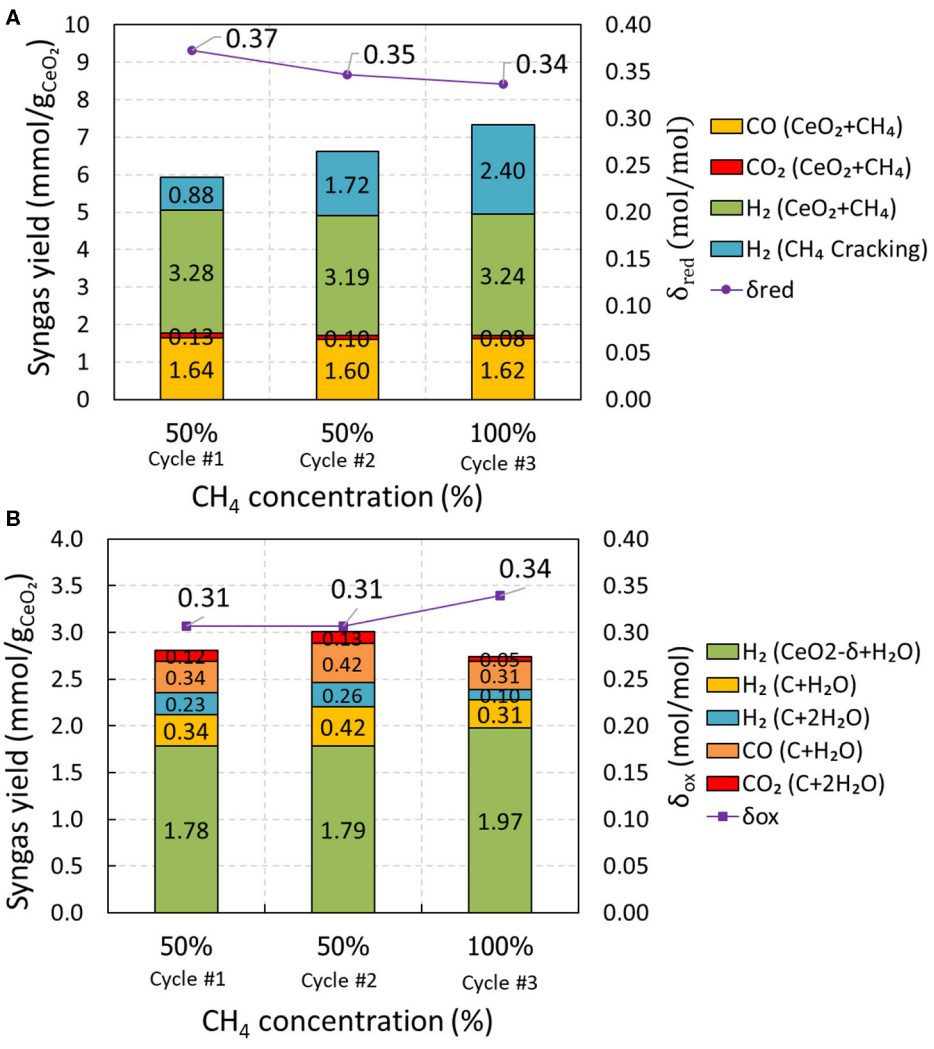

FIGURE 7 | Syngas yield and δ for **(A)** reduction and **(B)** oxidation of ceria foam cycled isothermally at 1,000°C as a function of inlet CH_4 concentration.

in H_2, associated with CH_4 cracking, was evidenced (2.40 $mmol/g_{CeO_2}$), presumably due to both overheating and higher CH_4 concentration. Furthermore, at 100% CH_4 concentration (cycle #3), a small increase in CO ($CeO_2 + CH_4$) and H_2 ($CeO_2 + CH_4$) yields was noticed when compared to 50% CH_4 concentration (cycle #2), demonstrating a positive impact on the main reaction. A slight change in CO ($CeO_2 + CH_4$) and CO_2 ($CeO_2 + CH_4$) yields led to similar δ_{red} (0.35 at cycle #2 *vs*. 0.34 at cycle #3). Therefore, increasing the CH_4 concentration may favor both the main reaction ($CeO_2 + CH_4$), as reflected by the improvement of CO (from $CeO_2 + CH_4$) and H_2 (from $CeO_2 + CH_4$) yields along with the side reaction (CH_4 cracking) as reflected by H_2 (from CH_4 cracking).

During the oxidation step (**Figure 7B**) at 50% CH_4 concentration, H_2 ($C + H_2O$), H_2 ($C + 2H_2O$), CO ($C + H_2O$), and CO_2 ($C + 2H_2O$) yields at cycle #2 were found to be higher than those from cycle #1 as expected, confirming a higher carbon deposition amount obtained during the reduction step, which was oxidized with H_2O. Besides that, the H_2 yield associated with the main reaction ($CeO_{2-\delta} + H_2O$) was stable [1.79 $mmol/g_{CeO_2}$ (cycle #2) *vs*. 1.78 $mmol/g_{CeO_2}$ (cycle #1)], leading to the same value of δ_{ox} (0.31). Importantly, the H_2 ($C + H_2O$), H_2 ($C + 2H_2O$), CO ($C + H_2O$), and CO_2 ($C + 2H_2O$) yields at cycle #3 were lower compared to those from cycle #2 even though the H_2 (cracking) yield was higher (**Figure 7A**). This is because of the decline of the oxidation temperature (below 1,000°C) that decreased the carbon deposition gasification reaction, leading to lower H_2 ($C + H_2O$), H_2 ($C + 2H_2O$), CO ($C + H_2O$), and CO_2 ($C + 2H_2O$) yields. On the other hand, a drop in the temperature during the oxidation step (cycle #3) positively influenced the exothermic reduced ceria oxidation with H_2O, leading to a higher H_2 ($CeO_{2-\delta} + H_2O$) yield (1.97 $mmol/g_{CeO_2}$). Moreover, at cycle #3, δ_{red} (0.34) exactly matched δ_{ox} (0.34), confirming a complete oxidation.

Figure 8 represents CH_4 conversion (X_{CH4}) and solar-to-fuel energy conversion efficiency ($\eta_{solar-to-fuel}$) for the three cycles at different CH_4 concentrations. As expected, the highest X_{CH4} was found at cycle #3 (46.79%) due to the higher impact of CH_4 concentration and CH_4 cracking reaction, followed by cycle #2 (40.78%) and cycle #1 (40.14%), in agreement with the trend of the syngas yield (**Figure 7A**). The $\eta_{solar-to-fuel}$ rose slightly with CH_4 concentration and exhibited the maximum (3.93%) at cycle #3. It was quite low as the solar power input was taken into account for both steps, including the duration of the reactor purging with Ar flow before switching to the oxidation step.

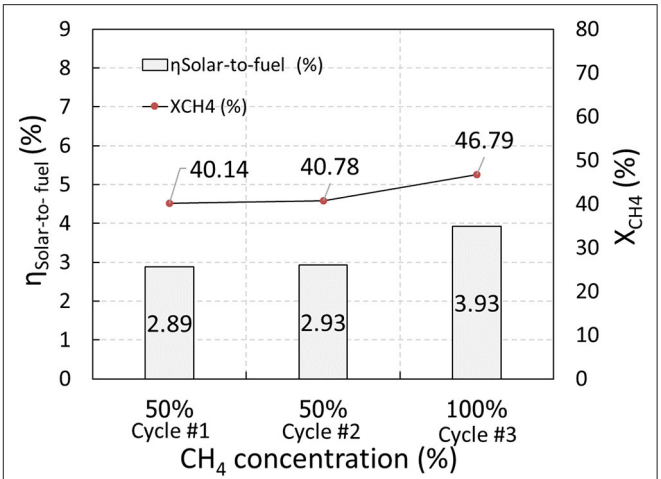

FIGURE 8 | CH_4 conversion and solar-to-fuel efficiency as a function of inlet CH_4 concentration at 1,000°C.

Effect of Methane Flow Rate

The impact of methane flow rate on syngas production from ceria foam [mass, 18.371g; annealed at 1,000°C (CeF-1000)] was studied for four cycles. **Figure 9** shows the influence of methane flow rate on the resulting syngas yields during ceria reduction with methane (**Figure 9A**), followed by ceria oxidation with H_2O (**Figure 9B**). The CH_4 flow rate was adjusted at 0.1, 0.2, 0.3, and 0.4 NL/min, together with a constant Ar carrier gas flow of 0.2 NL/min injected from the bottom inlet, resulting in CH_4 concentrations of 33.3, 50, 60, and 66.6% in the bottom gas flow.

During the reduction step (**Figure 9A**), the H_2 ($CeO_2 + CH_4$) and CO ($CeO_2 + CH_4$) yields increased moderately with CH_4 flow rate, from 3.25 and 1.66 $mmol/g_{CeO_2}$ at 0.1 NL/min to 3.78 and 1.89 $mmol/g_{CeO_2}$ at 0.4 NL/min, respectively, thereby enhancing the δ_{red} from 0.35 to 0.38. The CO_2 ($CeO_2 + CH_4$) yield was found to be stable in the range 0.08–0.10 $mmol/g_{CeO_2}$. Importantly, a sharp rise in the H_2 (CH_4 cracking) yield with CH_4 flow rate was observed, increasing from 0 at 0.1 NL/min (denoting the absence of the CH_4 cracking reaction) to 2.76 $mmol/g_{CeO_2}$ at 0.4 NL/min. This can be explained by the fact that the ceria reduction approached completion when the inlet CH_4 flow rate was increased, as reflected by δ_{red} that tended to level off at 0.38 above 0.2 NL/min. For these reasons, the rate of CH_4 supply exceeded the rate of oxygen released from the ceria structure, thereby leading to a favorable CH_4 cracking reaction. These phenomena usually happen when the rate of diffusion of the bulk lattice oxygen to the ceria surface is slower than methane dissociation, which leads to chemisorbed carbon being accumulated on the surface. In addition, the growth in the H_2 (CH_4 cracking) yield with CH_4 flow rate was in agreement with the growth of H_2 (CH_4 cracking) yield with CH_4 concentration, confirming that an increasing CH_4 concentration has an influence on CH_4 cracking reaction (**Figure 7A**).

During the oxidation step (**Figure 9B**), as expected the H_2 ($CeO_{2-\delta} + H_2O$) yield associated with the main reaction rose constantly with CH_4 flow rate, from 2.01 at 0.1 NL/min to 2.16 $mmol/g_{CeO_2}$ at 0.4 NL/min. This is due to the enhancement of the reduction extent during the reduction step that increased the oxygen vacancies. Consequently, the δ_{ox} was improved in the range 0.35–0.37 mol_O/mol_{CeO_2}. Regarding the resulting syngas yields associated with the side reactions, the H_2 ($C + H_2O$), H_2 ($C + 2H_2O$), CO ($C + H_2O$), and CO_2 ($C + 2H_2O$) yields increased with increasing CH_4 flow rate during the reduction step, from 0.01, 0.11, 0.01, and 0.11 $mmol/g_{CeO_2}$ at 0.1 NL/min to

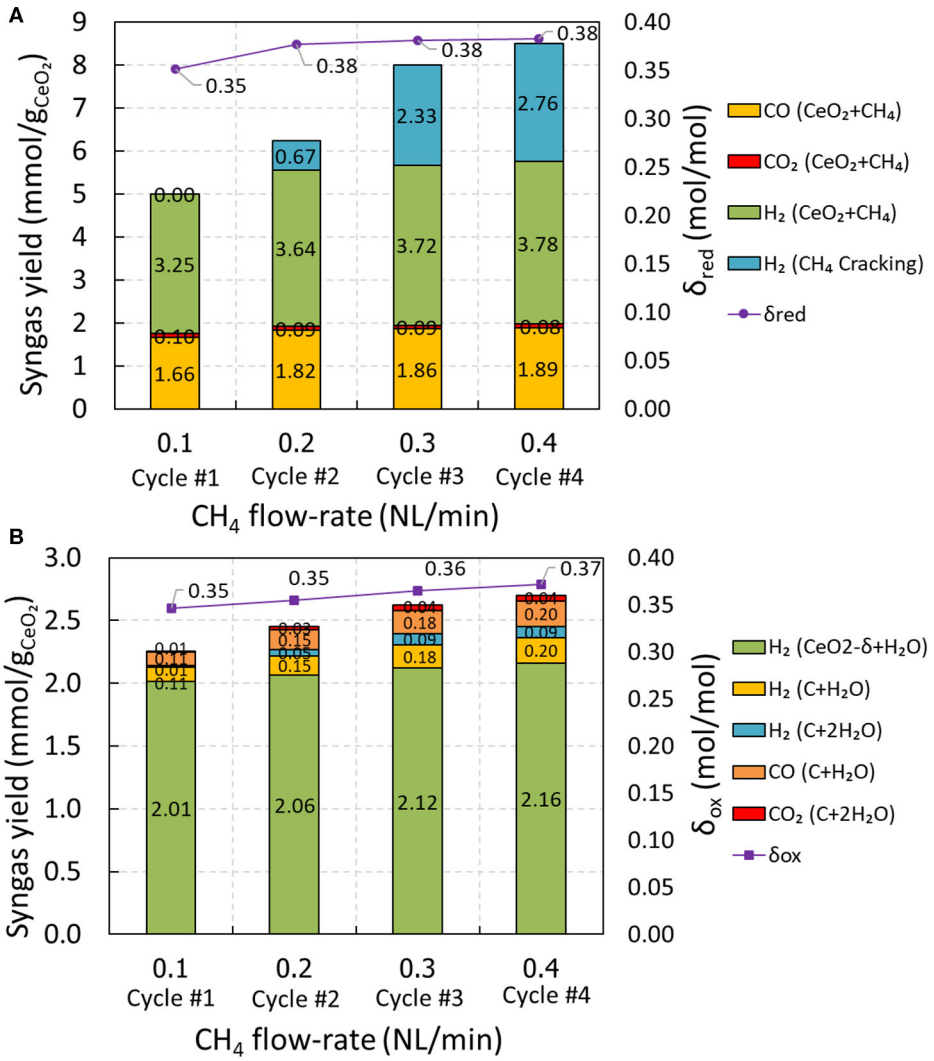

FIGURE 9 | Syngas yield and δ for **(A)** reduction and **(B)** oxidation of ceria foam cycled isothermally at 1,000°C as a function of inlet CH_4 flow rate.

0.04, 0.20, 0.09, and 0.20 mmol/g_{CeO_2} at 0.4 NL/min, respectively. This is attributed to the growth of solid carbon deposition caused by CH_4 dissociation with the increase of the CH_4 flow rate. However, this carbon can be gasified with H_2O, thus avoiding the issue of carbon remaining inside the reactor cavity receiver. For these reasons, increasing the methane flow rate enhances the extent of reaction and syngas yield; however, an excessive increase in the methane flow rate has a negative impact by increasing CH_4 dissociation, which results in the formation of CO and CO_2 during the oxidation step, thereby downgrading the H_2 purity.

The δ_{red} and δ_{ox} values were likewise similar for each tested CH_4 flow rate, indicating that the amount of oxygen being released and reversibly recovered is identical, thus again confirming complete reduced ceria re-oxidation with H_2O.

As expected, X_{CH4} declined with increasing CH_4 flow rate, from 68.52% at 0.1 NL/min to 53.82% at 0.4 NL/min, according to **Figure 10**. This is because the rate of CH_4 supply was higher than the rate of oxygen discharged by ceria reduction reaction. The X_{CH4} values reported here were comparable with those of previous studies [16−44% (Warren et al., 2020) and 13–60% (Krenzke et al., 2016)]. In addition, X_{CH4} was found to be dependent on the inlet methane flow rate. This is related to the methane cracking reaction, which resulted in solid carbon deposition. Therefore, an optimal trade-off in the inlet methane flow rate needs to be considered to maximize the methane conversion, which results in high syngas yield while minimizing the methane cracking side reaction. The $\eta_{solar-to-fuel}$ rose with the CH_4 flow rate and reached 5.6% at 0.4 NL/min, thanks to the improvement of the syngas yield with the CH_4 flow rate, as evidenced by **Figure 9**. The obtained $\eta_{solar-to-fuel}$ values were found to be typical with respect to the lab-scale solar reactors and comparable to previous studies (Warren et al., 2017; Fosheim et al., 2019). It is usual that the $\eta_{solar-to-fuel}$ values are lower than the theoretical ones predicted by thermodynamic

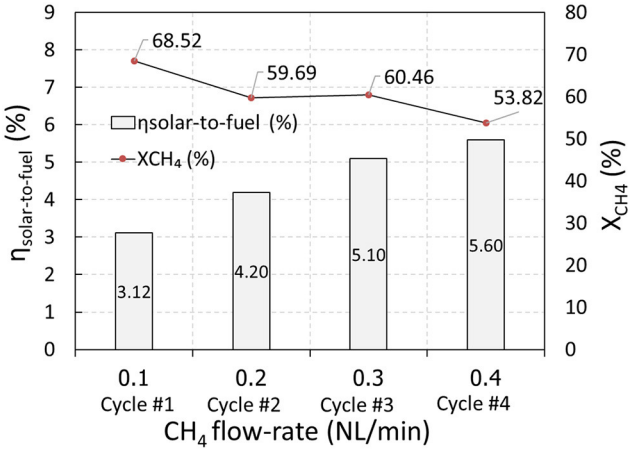

FIGURE 10 | CH_4 conversion and solar-to-fuel efficiency as a function of inlet CH_4 flow rate at 1,000°C.

analysis (Warren et al., 2017). The $\eta_{solar-to-fuel}$ can be potentially enhanced by scaling up the reactors to reduce heat losses, by optimizing heat and mass transfer inside the reactor and porous medium to improve the reaction rates and shorten the cycle duration (thereby lowering solar energy input), and by operating the process at optimal conditions to maximize the conversion of CH_4 and H_2O.

Influence of Ceria Annealing Temperature

The effect of annealing temperatures (1,000 vs. 1,400°C) of ceria foam on syngas yield was examined at a constant CH_4 flow rate of 0.2 NL/min with 50% CH_4 concentration during the reduction step and subsequently at a constant H_2O flow rate of 0.2 g/min with 55% H_2O concentration during the oxidation step. The syngas yield obtained from cycle #2 (CeF-1000) was compared to that obtained from cycle #1 (CeF-1400), as presented in **Figure 11**. It was found that during the reduction step (**Figure 11A**), the ceria foam CeF-1400 showed lower H_2 (CeO_2 + CH_4) and CO (CeO_2 + CH_4) yields than those for

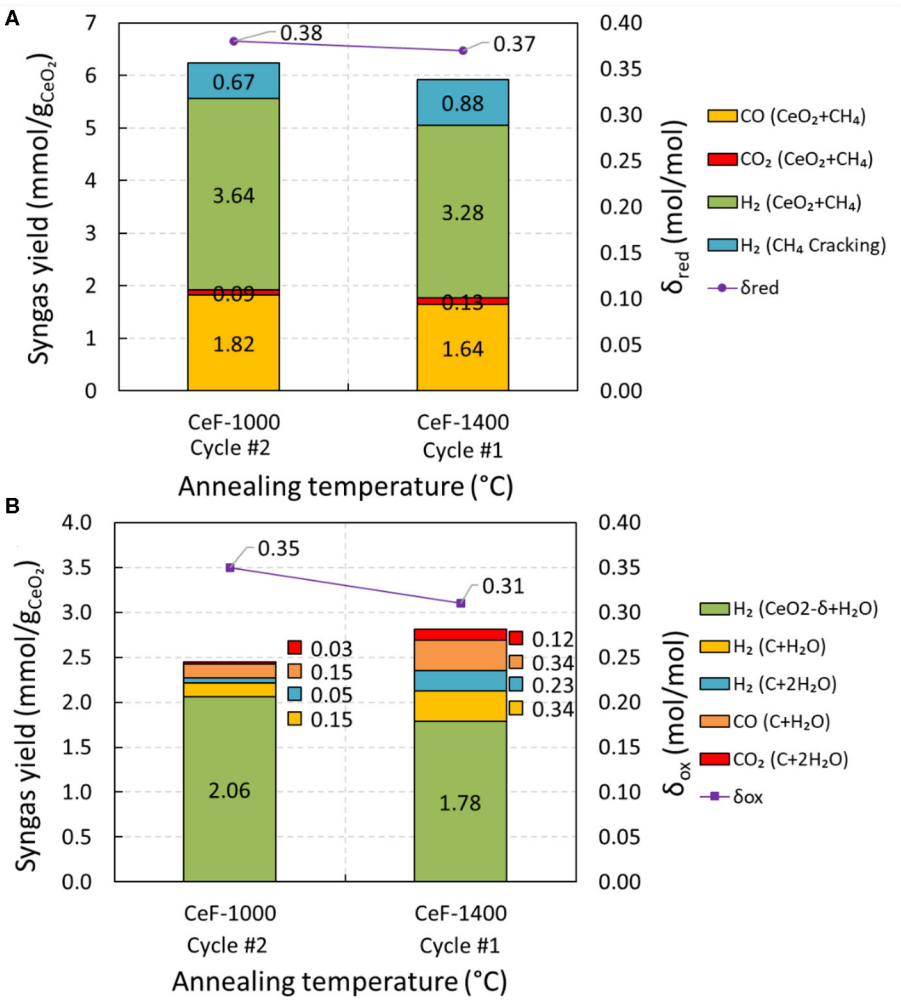

FIGURE 11 | Syngas yield and δ for **(A)** reduction and **(B)** oxidation of ceria foams cycled isothermally at 1,000°C as a function of annealing temperature.

CeF-1000, in turn resulting in a lower δ_{red} (0.37). Actually, the increasing annealing temperature (CeF-1400) resulted in the high densification of the ceria structure as evidenced by a decrease in density as well as porosity (**Table 1**), thereby leading to lower reduction extent and syngas yield. However, H_2 (CH_4 cracking) for CeF-1400 was higher (0.67 mmol/g_{CeO_2} for CeF-1000 vs. 0.88 mmol/g_{CeO_2} for CeF-1400). This is basically attributed to the longer reduction reaction duration for CeF-1400 (10-min duration for ceria mass 18.371 g of CeF-1000 vs. 30-min duration for ceria mass 30.963 g of CeF-1400), which provides an extended duration for the CH_4 cracking reaction to proceed.

Figure 11B, which is related to oxidation step, confirmed that the influence of CH_4 cracking reaction for CeF-1400 was higher when compared to CeF-1000, as evidenced by higher H_2 ($C + H_2O$), H_2 ($C + 2H_2O$), CO ($C + H_2O$), and CO_2 ($C + 2H_2O$) yields associated with the steam gasification of carbon. As expected, an increase in the annealing temperature significantly lowered the H_2 ($CeO_{2-\delta} + H_2O$) yield associated with steam ceria oxidation (e.g., from 2.06 mmol/g_{CeO_2} for CeF-1000 to 1.78 mmol/g_{CeO_2} for CeF-1400, in turn decreasing δ_{ox} from 0.35 to 0.31). For these reasons, it can be summarized that the annealing temperature of ceria foam should be as low as possible in order to increase its porosity, which promotes solid–gas reactions, thereby enhancing the reaction extent.

CONCLUSIONS

Chemical looping reforming of methane and H_2O splitting from isothermal ceria redox cycle for efficient syngas and hydrogen production have been assessed thermodynamically and experimentally. A 1.5-kW_{th} prototype volumetric reactor has been operated with real solar concentrated energy under isothermal conditions at 1,000°C, thereby demonstrating the technical feasibility and the reliability of the innovative and ecofriendly solar-driven methane reforming system for producing clean fuels. A parametric study considering the influence of inlet CH_4 concentration, CH_4 flow rate, and annealing temperature on syngas production rate, yield, foam-averaged oxygen non-stoichiometry (δ), CH_4 conversion, and reactor performance was performed. In agreement with thermodynamic predictions, syngas yield was produced with H_2/CO ratios approaching 2, along with undesired products regarding H_2O and CO_2 at the initial state of the reduction reaction. Increasing CH_4 concentration (50 and 100%) and CH_4 flow rate (0.1–0.4 NL/min) enhanced the reduction extent and syngas and hydrogen production yields during both steps, at the expense of a favorable CH_4 cracking reaction, which formed solid carbon deposition. However, the solid carbon is not detrimental to the whole process because carbon can be gasified with H_2O in the oxidation step (although producing CO and CO_2 and thus impacting the H_2 purity). In addition, a compromise temperature during the oxidation step should be considered, favoring exothermic reduced ceria oxidation while ensuring endothermic carbon deposition gasification with H_2O. Moreover, the sensitivity of the process to the temperature during on-sun testing was found to be significant, demonstrating that the transient conditions of a real solar-driven process need to be considered in scaling up the process. Increasing the annealing temperature of ceria foam had an adverse impact on its physical properties regarding density and porosity, leading to a decrease in the reduction extent and the syngas yield. Finally, solar-to-fuel conversion efficiency was in the range 2.9–5.6%, while CH_4 conversion in the range of 40.2–68.5% was achieved. Future work will aim at performing this process using renewable gaseous feedstocks such as biomethane, biogas, as well as biohythane for purely renewable (and carbon-neutral) fuel production.

DATA AVAILABILITY STATEMENT

The raw data supporting the conclusions of this article will be made available by the authors, without undue reservation.

AUTHOR CONTRIBUTIONS

All authors listed have made a substantial, direct and intellectual contribution to the work, and approved it for publication.

ACKNOWLEDGMENTS

King Mongkut's Institute of Technology Ladkrabang (KMITL), Thailand, and Campus France are gratefully acknowledged for scholarship support.

REFERENCES

Abanades, S., and Flamant, G. (2006). Thermochemical hydrogen production from a two-step solar-driven water-splitting cycle based on cerium oxides. *Sol. Energy*. 80, 1611–1623. doi: 10.1016/j.solener.2005.12.005

Bhosale, R. R., Takalkar, G., Sutar, P., Kumar, A., AlMomani, F., and Khraisheh, M. (2019). A decade of ceria based solar thermochemical H_2O/CO_2 splitting cycle. *Int. J. Hydrogen Energy* 44, 34-60. doi: 10.1016/j.ijhydene.2018.04.080

Chuayboon, S., Abanades, S., and Rodat, S. (2019b). Syngas production via solar-driven chemical looping methane reforming from redox cycling of ceria porous foam in a volumetric solar reactor. *Chem. Eng. J.* 356, 756–770. doi: 10.1016/j.cej.2018.09.072

Chuayboon, S., Abanades, S., and Rodat, S. (2020). Solar chemical looping reforming of methane combined with isothermal H_2O/CO_2 splitting using ceria oxygen carrier for syngas production. *J. Energy Chem.* 41, 60–72. doi: 10.1016/j.jechem.2019.05.004

Chuayboon, S., Abanades, S., and Rodat, S. (2019a). Stepwise solar methane reforming and water-splitting via lattice oxygen transfer in iron and cerium oxides. *Energy Technol*. doi: 10.1002/ente.201900415. [Epub ahead of print].

Chueh, W. C., Falter, C., Abbott, M., Scipio, D., Furler, P., Haile, S. M., et al. (2010). High-flux solar-driven thermochemical dissociation of CO_2 and H_2O using nonstoichiometric ceria. *Science* 330, 1797–1801. doi: 10.1126/science.1197834

Di, Z., Cao, Y., Yang, F., Zhang, K., and Cheng, F. (2019). Thermodynamic analysis on the parametric optimization of a novel chemical looping methane reforming in the separated productions of H_2 and CO. *Energy Convers. Manag.* 192, 171–179. doi: 10.1016/j.enconman.2019.04.046

Dincer, I., and Rosen, M. A. (2013). *Chapter 17 - Exergy Analysis of Hydrogen Production Systems*. eds I. Dincer, M. A. Rosen (Elsevier), 347–362.

Fosheim, J. R., Hathaway, B. J., and Davidson, J. H. (2019). High efficiency solar chemical-looping methane reforming with ceria in a fixed-bed reactor. *Energy* 169, 597–612. doi: 10.1016/j.energy.2018.12.037

Furler, P., Scheffe, J., Gorbar, M., Moes, L., Vogt, U., and Steinfeld, A. (2012). Solar thermochemical CO_2 splitting utilizing a reticulated porous ceria redox system. *Energy Fuels* 26, 7051–7059. doi: 10.1021/ef3013757

Furler, P., Scheffe, J., Marxer, D., Gorbar, M., Bonk, A., Vogt, U., et al. (2014). Thermochemical CO_2 splitting via redox cycling of ceria reticulated foam structures with dual-scale porosities. *Phys. Chem. Chem. Phys*. 16, 10503–10511. doi: 10.1039/C4CP01172D

Haeussler, A., Abanades, S., Jouannaux, J., Drobek, M., Ayral, A., and Julbe, A. (2019). Recent progress on ceria doping and shaping strategies for solar thermochemical water and CO_2 splitting cycles. *AIMS Mater. Sci.* 6, 657–684. doi: 10.3934/matersci.2019.5.657

Hathaway, B. J., Bala Chandran, R., Sedler, S., Thomas, D., Gladen, A., Chase, T., et al. (2015). Effect of flow rates on operation of a solar thermochemical reactor for splitting CO_2 via the isothermal ceria redox cycle. *J. Sol. Energy Eng.* 138:011007. doi: 10.1115/1.4032019

Krenzke, P. T., and Davidson, J. H. (2014). Thermodynamic analysis of syngas production via the solar thermochemical cerium oxide redox cycle with methane-driven reduction. *Energy Fuels* 28, 4088–4095. doi: 10.1021/ef500610n

Krenzke, P. T., Fosheim, J. R., and Davidson, J. H. (2017). Solar fuels via chemical-looping reforming. *Sol. Energy* 156, 48–72. doi: 10.1016/j.solener.2017.05.095

Krenzke, P. T., Fosheim, J. R., Zheng, J., and Davidson, J. H. (2016). Synthesis gas production via the solar partial oxidation of methane-ceria redox cycle: conversion, selectivity, and efficiency. *Int. J. Hydrogen Energy* 41, 12799–12811. doi: 10.1016/j.ijhydene.2016.06.095

Marxer, D., Furler, P., Takacs, M., and Steinfeld, A. (2017). Solar thermochemical splitting of CO_2 into separate streams of CO and O_2 with high selectivity, stability, conversion, and efficiency. *Energy Environ. Sci.* 10, 1142–1149. doi: 10.1039/C6EE03776C

Nair, M. M., and Abanades, S. (2016). Tailoring hybrid nonstoichiometric ceria redox cycle for combined solar methane reforming and thermochemical conversion of H_2O/CO_2. *Energy Fuels* 30, 6050–6058. doi: 10.1021/acs.energyfuels.6b01063

Nejat, P., Jomehzadeh, F., Taheri, M. M., Gohari, M., and Abd. Majid, M. Z. (2015). A global review of energy consumption, CO_2 emissions and policy in the residential sector (with an overview of the top ten CO_2 emitting countries). *Renew. Sustain. Energy Rev*. 43, 843–862. doi: 10.1016/j.rser.2014.11.066

Otsuka, K., Ushiyama, T., and Yamanaka, I. (1993). Partial oxidation of methane using the redox of cerium oxide. *Chem. Lett*. 22, 1517–1520. doi: 10.1246/cl.1993.1517

Otsuka, K., Wang, Y., and Nakamura, M. (1999). Direct conversion of methane to synthesis gas through gas–solid reaction using CeO_2-ZrO_2 solid solution at moderate temperature. *Appl. Catal. A Gen*. 183, 317–324. doi: 10.1016/S0926-860X(99)00070-8

Otsuka, K., Wang, Y., Sunada, E., and Yamanaka, I. (1998). Direct partial oxidation of methane to synthesis gas by cerium oxide. *J. Catal*. 175, 152–160. doi: 10.1006/jcat.1998.1985

Simakov, D. S. A., Wright, M. M., Ahmed, S., Mokheimer, E. M. A., and Román-Leshkov, Y. (2015). Solar thermal catalytic reforming of natural gas: a review on chemistry, catalysis and system design. *Catal. Sci. Technol*. 5, 1991–2016. doi: 10.1039/C4CY01333F

Warren, K. J., Reim, J., Randhir, K., Greek, B., Carrillo, R., Hahn, D. W., et al. (2017). Theoretical and experimental investigation of solar methane reforming through the nonstoichiometric ceria redox cycle. *Energy Technol.* 5, 2138–2149. doi: 10.1002/ente.201700083

Warren, K. J., and Scheffe, J. R. (2018). Kinetic insights into the reduction of ceria facilitated via the partial oxidation of methane. *Mater. Today Energy* 9, 39–48. doi: 10.1016/j.mtener.2018.05.001

Warren, K. J., and Scheffe, J. R. (2019). Role of surface oxygen vacancy concentration on the dissociation of methane over nonstoichiometric ceria. *J. Phys. Chem*. C 123, 13208–13218. doi: 10.1021/acs.jpcc.9b01352

Warren, K. J., Carrillo, R. J., Greek, B., Hill, C. M., and Scheffe, J. R. (2020). Solar reactor demonstration of efficient and selective syngas production via chemical looping dry reforming of methane over ceria. *Energy Technol*. doi: 10.1002/ente.202000053. [Epub ahead of print].

Welte, M., Warren, K., Scheffe, J. R., and Steinfeld, A. (2017). Combined ceria reduction and methane reforming in a solar-driven particle-transport reactor. *Ind. Eng. Chem. Res*. 56, 10300–10308. doi: 10.1021/acs.iecr.7b02738

Zheng, Q., Janke, C., and Farrauto, R. (2014). Steam reforming of sulfur-containing dodecane on a Rh–Pt catalyst: influence of process parameters on catalyst stability and coke structure. *Appl. Catal. B Environ.* 160–161, 525–533. doi: 10.1016/j.apcatb.2014.05.044

Zheng, Y., Wei, Y., Li, K., Zhu, X., Wang, H., and Wang, Y. (2014). Chemical-looping steam methane reforming over macroporous CeO_2-ZrO_2 solid solution: effect of calcination temperature. *Int. J. Hydrogen Energy* 39, 13361–13368. doi: 10.1016/j.ijhydene.2014.04.116

Zhu, X., Li, K., Wei, Y., Wang, H., and Sun, L. (2014). Chemical-looping steam methane reforming over a CeO_2-Fe_2O_3 oxygen carrier: evolution of its structure and reducibility. *Energy Fuels* 28, 754–760. doi: 10.1021/ef402203a

Conflict of Interest: The authors declare that the research was conducted in the absence of any commercial or financial relationships that could be construed as a potential conflict of interest.